JTTEE5 16:281–290
DOI: 10.1007/s11666-007-9032-9
1059-9630/$19.00 © ASM International

Effect of Feedstock Size and its Distribution on the Properties of Detonation Sprayed Coatings

P. Suresh Babu, D.S. Rao, G.V.N. Rao, and G. Sundararajan

(Submitted May 24, 2006; in revised form August 30, 2006)

The detonation spraying is one of the most promising thermal spray variants for depositing wear and corrosion resistant coatings. The ceramic (Al_2O_3), metallic (Ni-20 wt%Cr) , and cermets (WC-12 wt%Co) powders that are commercially available were separated into coarser and finer size ranges with relatively narrow size distribution by employing centrifugal air classifier. The coatings were deposited using detonation spray technique. The effect of particle size and its distribution on the coating properties were examined. The surface roughness and porosity increased with increasing powder particle size for all the coatings consistently. The feedstock size was also found to influence the phase composition of Al_2O_3 and WC-Co coatings; however does not influence the phase composition of Ni-Cr coatings. The associated phase change and %porosity of the coatings imparted considerable variation in the coating hardness, fracture toughness, and wear properties. The fine and narrow size range WC-Co coating exhibited superior wear resistance. The coarse and narrow size distribution Al_2O_3 coating exhibited better performance under abrasion and sliding wear modes however under erosion wear mode the as-received Al_2O_3 coating exhibited better performance. In the case of metallic (Ni-Cr) coatings, the coatings deposited using coarser powder exhibited marginally lower-wear rate under abrasion and sliding wear modes. However, under erosion wear mode, the coating deposited using finer particle size exhibited considerably lower-wear rate.

Keywords Al_2O_3, fracture toughness, Ni-Cr, thermal spray, tribological properties, WC-Co

1. Introduction

In recent years, thermal spray techniques successfully emerged as the most popular technique for depositing thick coatings to combat various forms of wear and corrosion (Ref 1-3). In all thermal spray variants, powder particles are utilized as the feedstock. Thermal spray grade powders of wide variety with respect to composition and the powder manufacturing route are commercially available. However, the particle size distribution of the commercially available thermal spray powders have much less variation with the particle size range being 30-110 μm in the case of plasma spray grade and from 10 to 44 μm in the case of HVOF spray grade.

In view of the above, a natural question to ask is whether the powder size distribution available in commercial powders are adequate or a further narrowing of powder particle size distribution is of any benefit in terms of improved performance of the resulting coatings. However, it is to be noted that production of powder feedstock using a narrower powder particle size distribution than that currently used commercial powders will entail a higher cost and therefore the improvement in coating performance has to be substantial.

Earlier work in this area had been quite limited. Peterson et al. (Ref 4) noted a significant increase in coating density and hardness when they carried out air plasma coatings with HVOF grade powder having a powder particle size in the range 10-44 μm as opposed to conventional plasma grade powder of larger powder particle size (10-105 μm). However, these authors did not utilize powder grades finer than HVOF grade as done in the present study. Berget et al. (Ref 5, 6) found that HOVF coatings with a narrower size range of WC-Co-Cr powders, exhibited superior erosion resistance. In contrast, Li et al. (Ref 7) noted a degradation in the high-temperature corrosion performance of HVOF MCrAlY coatings at lower-powder particle sizes due to the fact that the oxide inclusion content in the coatings with finer powders were much higher. In the case of plasma sprayed hydroxyapatite (HA) coatings (Ref 8), it was observed that use of finer HA powder (20-45 μm) resulted in lower porosity and lower proportions of unmelted particles but caused an increase in the undesirable amorphous phase as compared to using the coarser HA powder (45-53 μm).

Given the limited data on the influence of the powder particle size on the coating properties and performance, it was felt that there is a need for a detailed study of this aspect. In view of the above, in the present study, the influence of the feedstock powder particles size on a variety of coating properties (coating roughness, porosity,

P. Suresh Babu, D.S. Rao, G.V.N. Rao, and **G. Sundararajan,** International Advanced Research Center for Powder Metallurgy and New Materials (ARCI), Balapur (P.O), Hyderabad, 500 005, India. Contact e-mail: gsundar@arci.res.in.

phase content, hardness, toughness, and wear resistance) has been evaluated for three types of coatings namely the ceramic Al_2O_3, metallic Ni-20%Cr, and cermet WC-12%Co. All the coatings have been carried out using the detonation spray coating (DSC), which is a variant of the HVOF process.

2. Experimental Procedure

2.1 Feedstock Characterization

In the present study, the commercially available Al_2O_3 (HVOF grade, H.C. Starck, Germany), Ni-20%Cr (HVOF grade, H.C. Starck, Germany) ,and WC-12%Co (HVOF grade, Sultzer Met Co.,USA) powders were used. Particle size analyzer (CILAS-920, France) was utilized to carry out the particle size analysis of each of the three powders before and after classification. In house fabricated centrifugal air classifier was employed for separating the finer and coarser fractions from above powders with relatively narrow size distribution. Henceforth, the coarse fractions of Al_2O_3, Ni-20%Cr, and WC-12%Co powders are referred to as coarse WC-Co, coarse Al_2O_3, and coarse Ni-Cr respectively while the fine fractions are referred as fine WC-Co, fine Al_2O_3, and fine Ni-Cr. The original as received powders with a wide particle size distribution are henceforth referred to as ''as received''. The scanning electron microscope (SEM, S-4300SE/N, Hitachi, Japan) was employed for observing the particle morphology and size distribution. An x-ray diffractometer (XRD, ADX D8, Bruker, Germany, Cu-K_α radiation, 40 kV, 40 mA, 0.02°/s, scan rate) was utilized to identify the phases present in the powders.

2.2 Coating Deposition

The coatings were deposited using the detonation spray process. The configuration of the deposition system employed is described elsewhere (Ref 9). The coatings were deposited onto the grit-blasted mild steel substrates using the previously optimized spray conditions (Ref 10-12) as illustrated in Table 1. The coating deposition was continued till a final coating of thickness 325 ± 25 μm was reached. The spray parameters for a given type of powder were kept identical for all size fractions.

2.3 Coating Characterization

The surface roughness (R_a) of the as-sprayed coatings was measured using surface roughness measuring gauge (SURTRONIC-3+, UK). The coated samples were sectioned and mounted using bakelite for carrying out metallographic studies. The porosity of coatings was measured using a metallurgical microscope attached with an image analyzer system (Image Pro Plus, Media Cyber Netics, USA). The Vickers microhardness of the coatings was measured using Vickers microhardness tester (Leitz-112473, Germany) at 300 g load. For each coating, at least 10 measurements were made on the coating cross section and the calculated mean value is being reported. The XRD analysis was carried out to identify the phases present in the coatings as well. The SEM examination was carried out for evaluating the coating morphology and %porosity.

The indentation fracture toughness of WC-Co and Al_2O_3 coatings were evaluated by carrying out indentations on these coatings at loads of 10 and 1.5 kg respectively using a Vickers indenter. At least five indents were made for each coating. Special care was taken to ensure that one diagonal of the Vickers indenter was parallel to the coating-substrate interface and that the indent was situated along the centerline of the coating cross section. The SEM images of these indentations were taken and the crack lengths were measured using image analysis. The fracture toughness (K_C) of the coatings was then evaluated using the Evans and Charles equation (Ref 13). However, in the case of Ni-Cr coatings, indentation fracture toughness could not be estimated due to the fact that even at highest load of 30 kg, cracks did not develop at the indentation corners due to high toughness of Ni-20Cr coatings.

The abrasive wear resistance of the coated samples was evaluated using a dry sand-rubber wheel abrasion test rig (ASTM G65). Silica particles (angular, 200±20 μm) were used as the erodent medium. The specimens were cleaned ultrasonically with acetone and weighed before and after each test. A normal load of 5 kg was used for WC-12%Co and Al_2O_3 while 1 kg was employed for Ni-Cr coatings. The test was continued up to 2000 revolutions. However, the weight loss of the samples was measured after every 200 revolutions.

The sliding wear tests were performed using a pin-on-disc test rig (ASTM G99). The coated pins slid against the sintered WC-Co disc (HV = 1750) under a nominal pressure of 1.7 MPa in case of WC-12%Co and Al_2O_3 coated pins. For Ni-Cr coated pins a nominal pressure of 0.35 MPa was used. A constant sliding velocity of 4.50 m/s was employed for all the coatings. The weight loss of the pin was measured after every killometer sliding distance and test was continued for a total sliding distance of 6 km.

The room temperature solid particle erosion tests (ASTM G76) were carried out at two different impact angles (90° and 30°) and at a particle velocity of 60 m/s. Silica particles (angular, 200 ± 20 μm) were used as an erodent medium. The erosion tests were carried out for a total duration of 40 min. However, after every 5 min, the weight loss of the samples was measured. The erosion rate (E), i.e., the ratio of sample weight loss to the weight of the erodent causing the loss was calculated after each weight loss measurements. The density of each coating was measured using the Archimedes principle. The weight

Table 1 Parameters used for obtaining the coatings by DSC

Parameter	Al_2O_3	Ni-20%Cr	WC-12%Co
Oxygen flow, L/h	4800	2640	2800
C_2H_2 flow, L/h	1920	2400	2400
N_2 flow, L/h	720	960	1040
Spray distance, mm	200	165	165
O_2/C_2H_2 ratio	2.5	1.1	1.16

loss data obtained under abrasion, erosion, and sliding wear modes were converted to volume loss using density data so as to obtain volumetric wear rates.

3. Results and Discussions

3.1 Powder Characterization

3.1.1 Powder Morphology and Size Distribution. The SEM images of Al_2O_3, Ni-Cr and WC-Co powders pertaining to as received, fine and coarse fraction are depicted in Fig. 1. The Al_2O_3 and WC-12Co powder particles are irregular and angular in shape consistent with the fact that they were manufactured using the sintering followed by crushing. The Ni-Cr powder particles also exhibiting angular and blocky morphology as it has been obtained using water atomization route. Figure 2 shows the cumulative particle size distribution curves including particle size at 50% (d_{50}) and particle size at 90% (d_{90}) values of coarse, fine and as received powders. As is evident from the powder morphology illustrated in Fig. 1 and size distribution provided in Fig. 2, the effectiveness of centrifugal air classifier to handle the powders of wide range with regard to density and to separate them in to narrow size distribution powders has been demonstrated. Among all the powders, the Al_2O_3 powders exhibited the finest particle size.

3.1.2 Phase Identification. The XRD analysis was carried out on Al_2O_3, Ni-20Cr and WC-12Co powders and is presented in Fig. 3. The α-Al_2O_3 is the only phase identified in Al_2O_3 powder. The powder pattern of Ni-Cr exhibited three major peaks responsible for Ni-Cr (111), (200) and (220) indicating that the powder exists in FCC phase and Cr is in solid solution in a Ni matrix. In case of WC-Co powder, only WC and Co phases were identified. In addition, for a given powder, the phases identified were the same irrespective of whether the powders were as received or classified.

3.2 Coating Characterization

3.2.1 Surface Roughness. The surface roughness (R_a) values measured on all the coatings are presented in Fig. 4. As a rule, the surface roughness of the coatings increases with increasing the average powder particle size used as the feedstock. Of the three coatings, the Al_2O_3 coatings exhibited the lowest surface roughness values while the Ni-Cr coatings have the highest surface roughness. The lowest roughness of the Al_2O_3 coatings can be explained on the basis that Al_2O_3 powders used to form the coatings had the finest powder particle size values. Though WC-Co and Ni-Cr powder particles have the similar sizes, the roughness is lower for WC-Co coatings mainly due to the selective softening and flow of the Co phase during the coatings process which results in efficient filling of the pores.

3.2.2 Coating Microstructure. Figure 5 illustrates the microstructural details of all the coatings. From Fig. 5, it is evident that the porosity levels increased with an increase in the average size of the powder particles utilized to deposit the coatings. The observation is consistent with

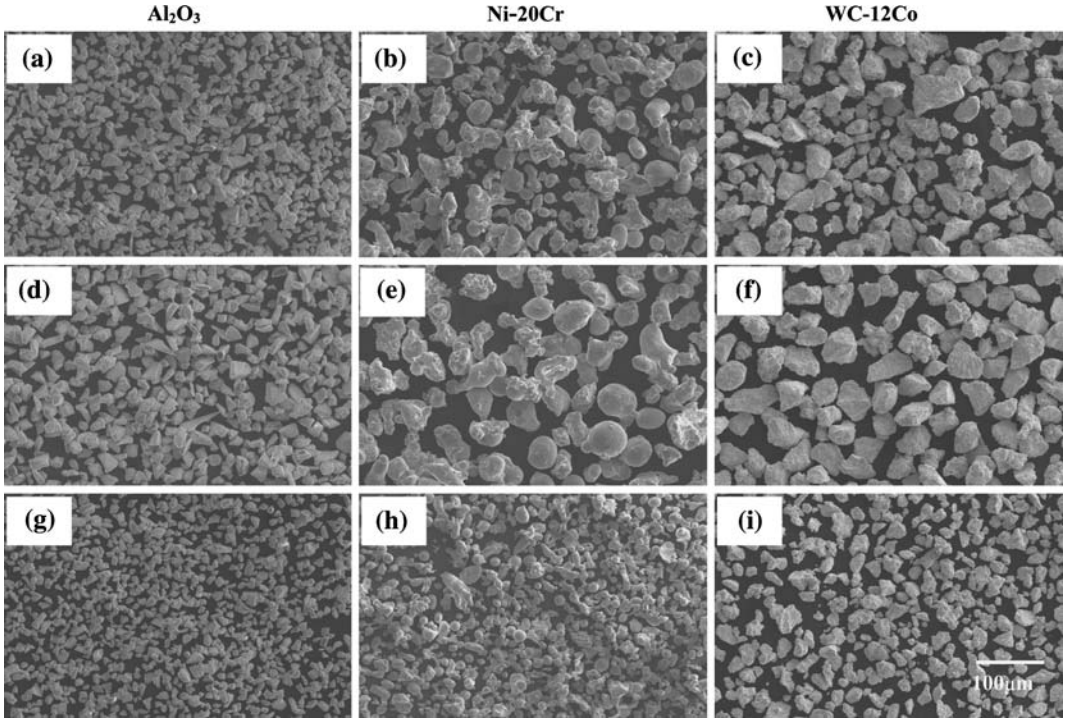

Fig. 1 SEM images of Al_2O_3, Ni-20Cr and WC-12Co powders. (a-c)—as received; (d-f)—coarse; (g-i)—fine fractions of respective powders

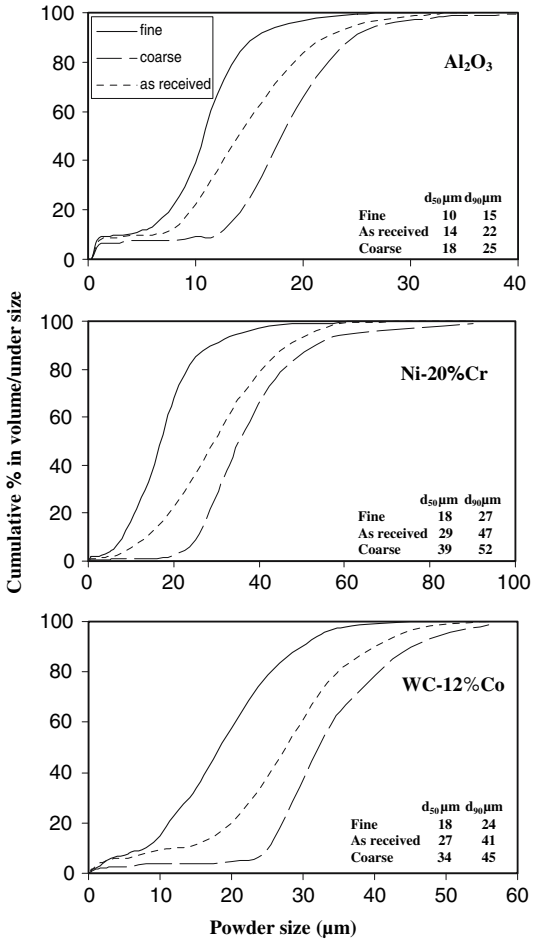

Fig. 2 Cumulative size distribution curves of Al_2O_3, Ni-Cr, and WC-Co powders

results reported in earlier studies (Ref 4, 14, 15). The first observation to be made is that the quantitative porosity data shown in Fig. 6 is consistent with the trends in porosity observed on the coating cross section (Fig. 5). The influence of powder particle size on porosity is most dramatic in the case of Ni-Cr coatings. As discussed in the last section, the absence of binder phase in Ni-Cr coatings which usually facilitates closure of pores inconjuction with relatively large powder particle size (as compared to Al_2O_3) leads to larger pores more closely related to particle size leading to such a strong relationship between porosity volume and powder particle size in Ni-Cr coatings. Even though the porosity levels are substantially lower in Al_2O_3 coatings due to finer powder particle sizes, the strong relationship between powder particle size and porosity is still evident and this is again due to absence of binder phase in Al_2O_3 coatings. In contrast, in the case of WC-Co coatings the presence of the cobalt binder phase not only reduces the extent of porosity as corresponding to Ni-Cr coatings formed using powder particle size range nearly the same as WC-Co powders, but also does not lead to a strong relationship between powder particle size and porosity due to additional filling of pores by the Co phase which has a lower-melting point.

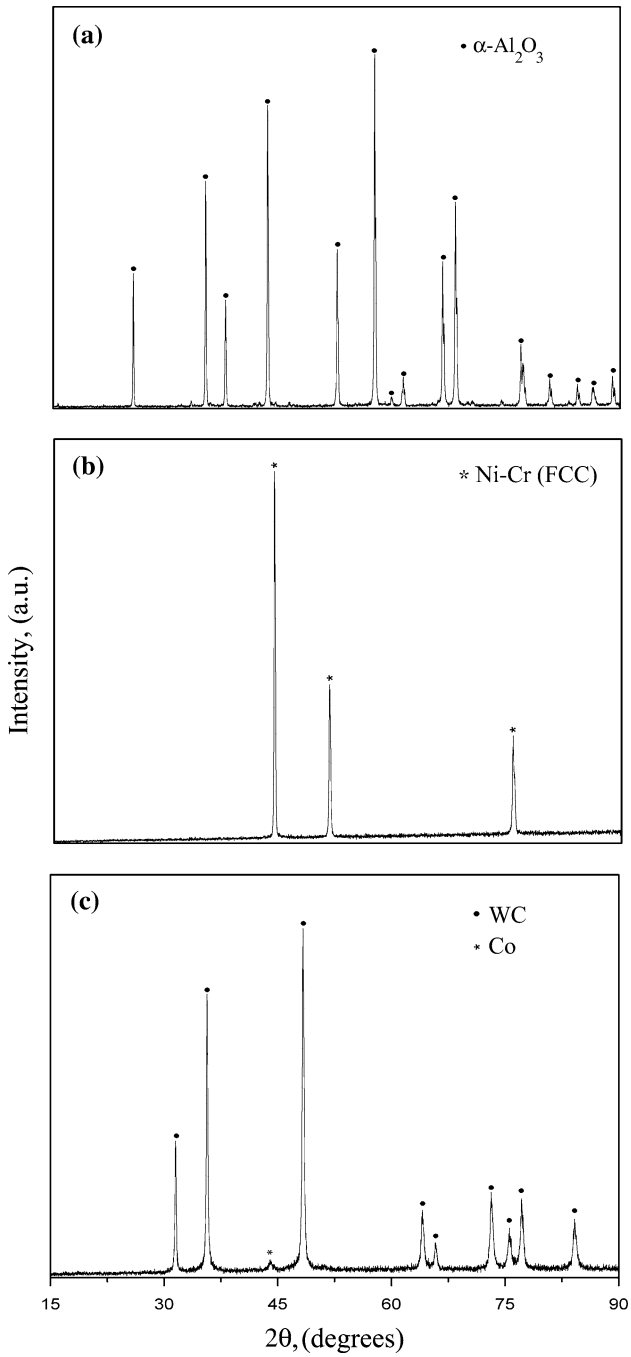

Fig. 3 XRD patterns of (a) Al_2O_3 (b) Ni-20Cr, and (c) WC-12Co powders

3.2.3 Phase Analysis. The XRD analysis was carried out on all coatings to identify the phases present in the coatings. The x-ray diffraction patterns of sprayed coating of three size ranges of Al_2O_3 coatings are shown in Fig. 7(a). It is well known that the metastable phases form during Al_2O_3 spray deposition due to rapid solidification in all variants of thermal spray techniques (Ref 10, 16-19). Consequently, in addition to α-Al_2O_3, which is the only phase present in the starting powder, the coatings also

exhibited substantial amount of γ-Al_2O_3 phase as well. The quantitative phase analysis showed that the volume percent of % γ-Al_2O_3 increased with decrease in the powder particle size of Al_2O_3 coatings as illustrated in Fig. 7(b). The change in the amount of metastable γ-Al_2O_3 as a function of feed stock powder size at identical

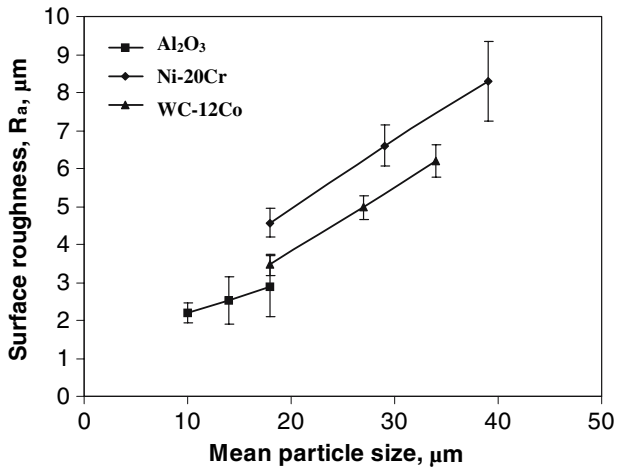

Fig. 4 Surface roughness (R_a) of as-sprayed Al_2O_3, Ni-20Cr, and WC-12Co coatings

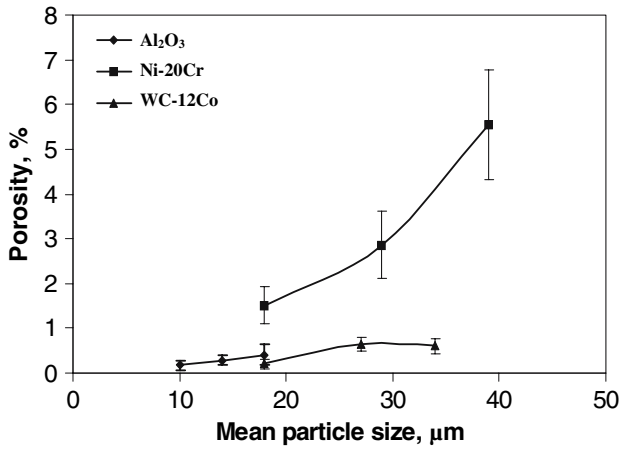

Fig. 6 Porosity of detonation sprayed Al_2O_3, Ni-20Cr and WC-12Co coatings

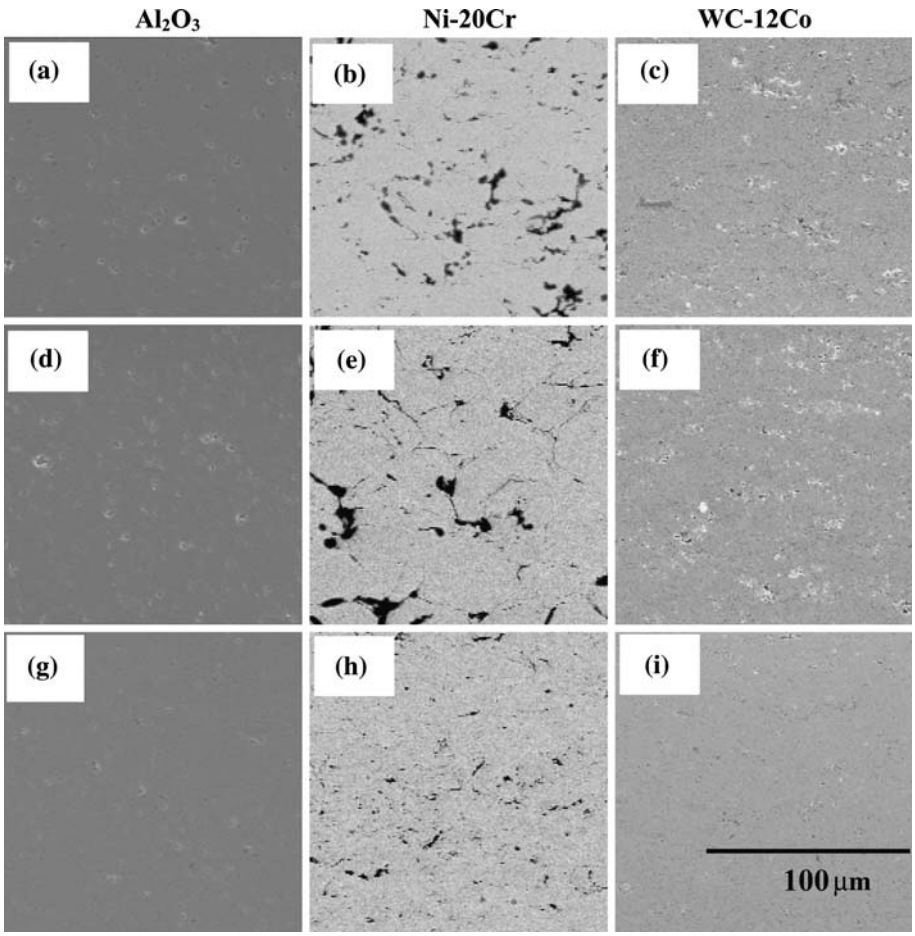

Fig. 5 SEM images of detonation sprayed Al_2O_3, Ni-20Cr and WC-12Co coatings deposited using (a-c)—as received; (d-f)—coarse; (g-i)—fine fractions of respective powders

spraying conditions in the present study is believed to be due to different degrees of melting of fine and coarse size particles and also due to higher cooling rates experienced by finer particles on solidification. The spreading and crystallization of Al_2O_3 liquid droplets on impact with substrate have been analyzed extensively in the case plasma and flame spray deposition processes. These studies suggest that if the liquid droplets flatten completely before crystallization, γ-Al_2O_3 is homogeneously nucleated from the molten droplet because the energy barrier is less for γ-Al_2O_3 nucleation than that of α-Al_2O_3. Particles that are not completely molten crystallize to α-Al_2O_3 from preexisting nuclei (Ref 16, 18). However, detailed study of liquid droplet solidification and nucleation kinetics is out of scope in this present study. But, under identical deposition conditions, finer particles get heated up quickly and also to higher temperatures compared to coarser particles. As a result, under identical process conditions, finer particles are more likely to be molten leading to higher γ-Al_2O_3 volume fraction.

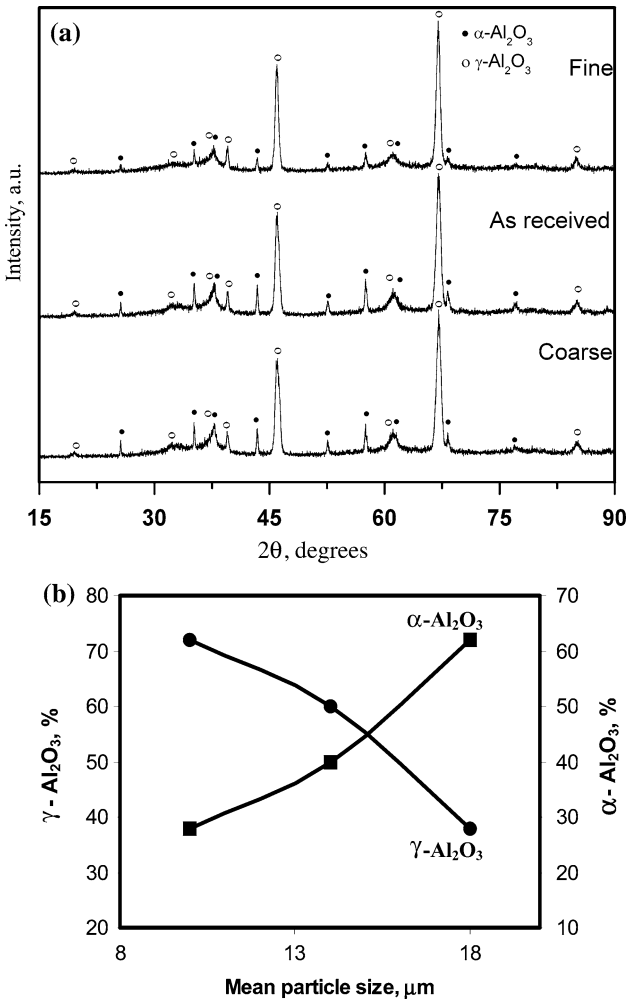

Fig. 7 X-ray diffractions patterns (a) and phases present as a function of feedstock size (b) of Al_2O_3 coatings

The x-ray diffraction patterns of WC-Co coatings are shown in Fig. 8(a). It can be clearly observed that the decomposition of WC phase has taken place during the coating process. Along with WC, Co phases, which are the only phases present in the starting powder, the other phase like W_2C and mixed cobalt carbide phases are observed in all the coatings. The slightly broader peak at $2\theta \sim 43°$ corresponds to mixed cobalt carbides. A closer look reveals that this hump can also be attributed either to the amorphous/nanocrystallinity of coatings or due to larger strain, developed due to severe deformation/impact during the coating deposition (Ref 20). However, the peaks corresponding to W_2C are most pronounced in the fine WC-Co coatings. The amount of WC and W_2C phases present in the coatings as function of average powder particle size is plotted and shown in Fig. 8(b). The extent decomposition of WC has increased with a decrease in the average powder particle size. It has been reported earlier that in the case of thermal spray WC-Co coatings, the degree of decomposition of WC increases with increase in particle temperature (Ref 21-23). In the thermal spray variants like plasma and HVOF processes, free tungsten phase is often found (Ref 21, 24). However, there is no free tungsten observed in the present study. This clearly

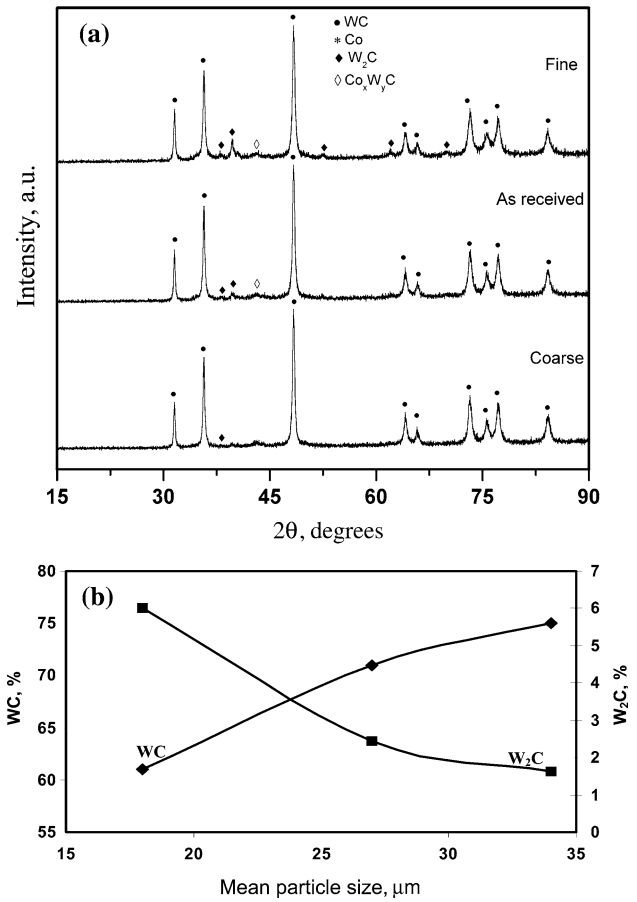

Fig. 8 X-ray diffractions patterns (a) and phases present as a function of feedstock size (b) of WC-12Co coatings

indicates that the degree of decomposition of WC-Co coatings is considerably lower in the detonation spray process as compared to air plasma spray and plasma spray processes. From the above discussion, it is clear that under the identical deposition conditions, powder particle size has a substantial influence on the phase formation in the case of Al_2O_3 and WC-Co coatings.

The x-ray diffraction patterns of Ni-Cr coatings are shown in Fig. 9. In contrast to the phase changes associated with in Al_2O_3 and WC-12%Co coatings, no phase change is observed during spraying of Ni-Cr powders. As in the case of powders, the three prominent peaks seen for the as-sprayed coatings are indexed to the Ni-Cr FCC phase. However, the only difference is that the XRD peaks are much broader in the case of coatings as compared to the powder pattern. Such a peak broadening is attributed to the lattice distortion that occurs during the splat formation in the spray process. Similar peak broadening phenomenon has been observed in the case of HVOF sprayed Ni-Cr coatings (Ref 25).

3.2.4 Microhardness of Coatings. The variation of microhardness with mean powder particle size for all the three coatings are presented in Fig. 10. In the case of Al_2O_3 coatings, the hardness of the coating increases with increasing powder particle size. The above behavior can be rationalized on the basis that the γ-Al_2O_3 volume fraction decreases with increasing particles size since earlier work (Ref 26) has clearly established that γ-Al_2O_3 is considerably softer than α-Al_2O_3. In contrast to the behavior of Al_2O_3 coatings, the hardness of Ni-Cr coating decreases steadily with increasing mean powder particle size. The earlier work by other investigators with plasma sprayed Al_2O_3-TiO_2 coatings (Ref 27) and 3Y-TZP ceramics (Ref 28) have clearly demonstrated that a change in porosity levels from 1 to 5% or so can reduce the hardness of the coating substantially. However, there no literature data is available on the influence of porosity of Ni-Cr coatings on their hardness. As a result it can be concluded that decrease in the hardness of Ni-Cr coatings with increasing particle size is most likely due to the increased porosity levels. Finally, in the case of WC-Co coatings, the hardness is not particularly influenced by powder particle size. It is known that the W_2C phase is harder than the WC phase and on that basis the hardness of WC-Co should increase with decreasing powder particle size since the volume fraction of W_2C phase in the WC-Co coating increases with decreasing powder particle size (see Fig. 8b). However the dissociation of WC to W_2C phase (i.e., decarburazation) is expected to result in a decrease in the volume fraction of total carbides in the coating (Ref 21-24, 29) and this effect most probably compensates for the increase in hardness due to W_2C formation leading to a net negligible effect of particle size on hardness of WC-Co coatings.

3.2.5 Fracture Toughness of Coatings. The influence of powder particle size on the indentation toughness (K_C) of the Al_2O_3 and WC-Co coatings are illustrated in Fig. 11. In the case of Al_2O_3 coatings, the K_C value decreases substantially with increasing powder particle size. Such a behavior is most probably due to the fact that

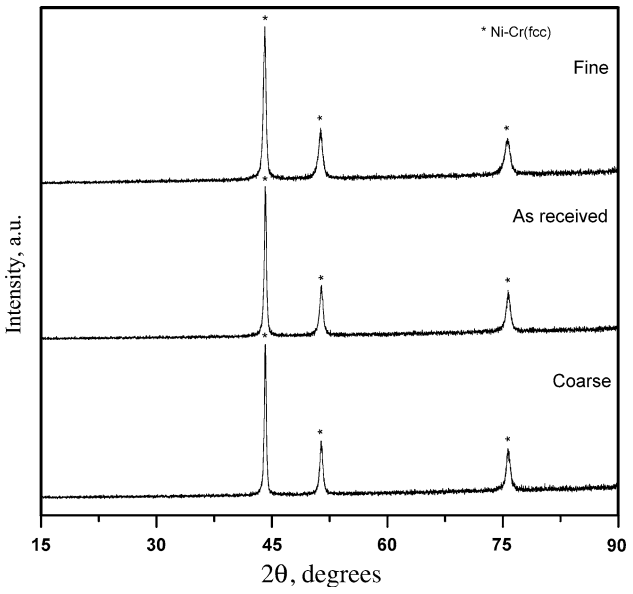

Fig. 9 X-ray diffractions patterns of Ni-Cr coatings

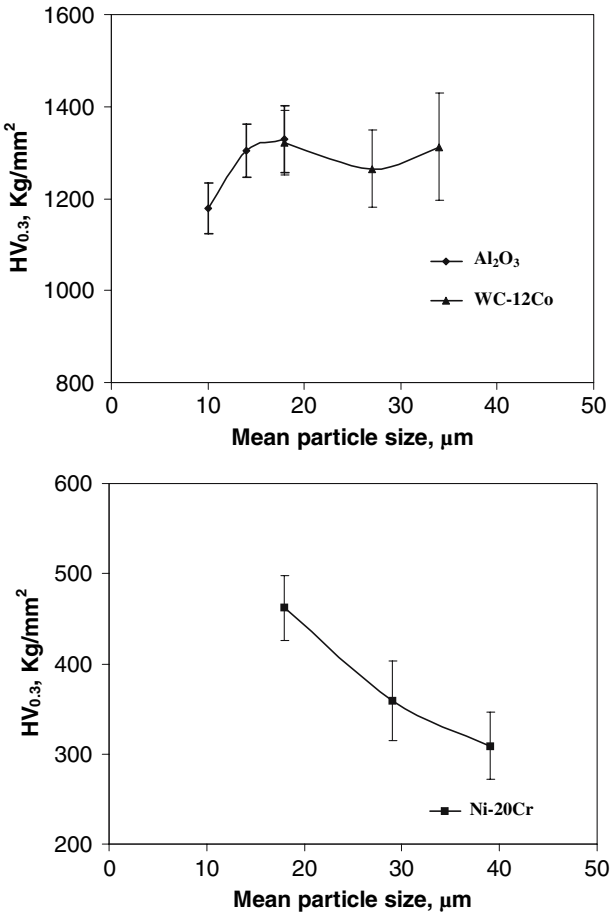

Fig. 10 Microhardness of detonation sprayed Al_2O_3, Ni-20Cr, and WC-12Co coatings

the volume fraction of γ-Al_2O_3 phase, which is the softer phase compared α-Al_2O_3 and therefore likely to be tougher (no literature data exists on the toughness of γ-Al_2O_3) and decreases substantially with increasing powder particles size (see Fig. 7b). The toughness of the WC-Co coating on the other hand increased with increasing powder particle size. It is generally accepted that the indentation toughness of WC-Co depends on WC cuboid size and the inter cuboid spacing (Ref 30). A detailed SEM examination (in backscatter mode) of the WC-Co coatings in the present case as shown in Fig. 12, indicates that the WC cuboid size ($0.8 \pm 0.3\mu m$) is identical in the as received, fine and coarse WC-Co coatings. Thus, it can be concluded that WC cuboid size cannot be correlated with the observed variation of toughness with powder particle size. A more reasonable explanation can be in terms of the decomposition of WC since W_2C phase is harder but more brittle than WC phase. Since the volume fraction of the brittle W_2C phase decreases with increasing powder particle size (see Fig. 8b), the corresponding increase in indentation toughness can be explained.

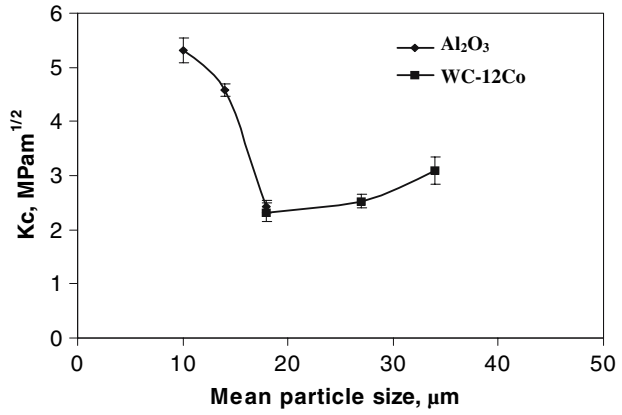

Fig. 11 Fracture toughness of detonation sprayed Al_2O_3 and WC-12Co coatings

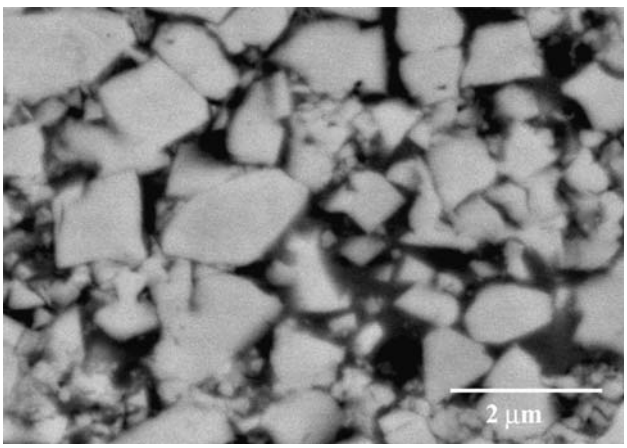

Fig. 12 BSE image, revealing the size distribution of WC cuboids in the as received WC-Co coating

3.2.6 Wear Behavior. The abrasion, sliding and erosion rates of the three coatings as a function of mean particle size are illustrated in Fig. 13(a-c). In the case of Al_2O_3 coatings, the abrasion and sliding wear rate decreases with increasing particle size. Such a behavior implies that increased hardness of the Al_2O_3 coatings with increasing particle size has a dominant effect on abrasion and sliding as compared to fracture toughness which actually decreases with increasing particle size (Fig. 11). In contrast, under erosion conditions, the hardness as well as toughness of the Al_2O_3 coatings appear important since an optimum correlation of hardness and toughness at intermediate particles size provides the best erosion resistance at both impact angles (Fig. 13c). At a more fundamental level, the increase in the hardness and decrease in toughness of the Al_2O_3 coatings with increasing particle size is essentially due to the fact that the proportion of the harder and less tough α-Al_2O_3 phase in the Al_2O_3 coating increases with increasing particle size (Fig. 7).

In the case of WC-12Co coatings, the sliding, abrasion and erosion wear rates increase with increasing particle size (see Fig. 13), where as the hardness of WC-Co coating

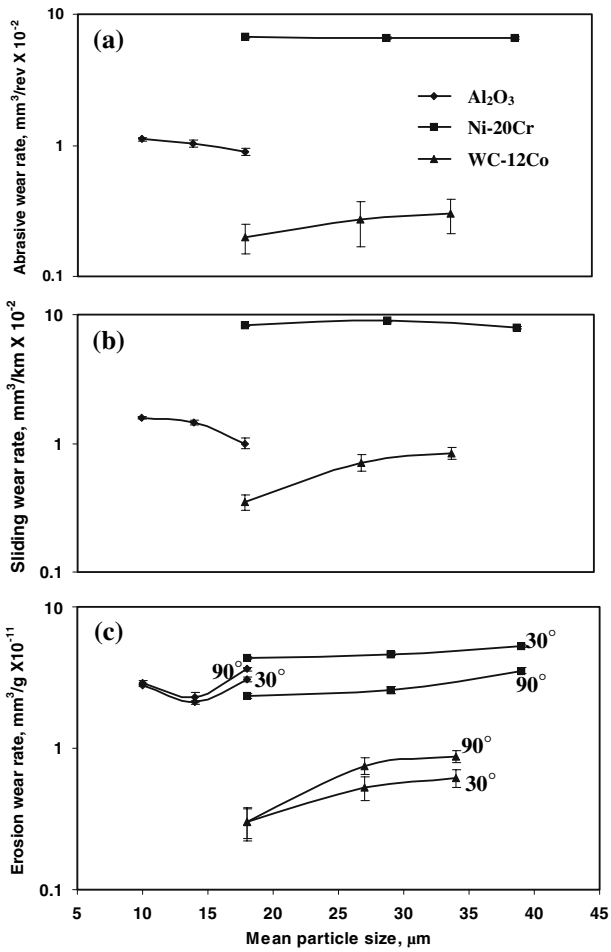

Fig. 13 Wear performance of Al_2O_3, Ni-Cr, and WC-Co coating as a function of mean particle size

is only marginally affected by the particle size (Fig. 10) and the toughness increased with increasing particle size (Fig. 11). In general, with the same hardness value, higher fracture toughness should yield lower-wear rate. However, the results obtained in the present study do not clearly follow the above trend. The reason for such a behavior is not clear and requires a more detailed investigation.

The considerably higher toughness of Ni-20Cr coatings as compared to Al_2O_3 and WC-Co coatings has precluded the measurement of its toughness using the indentation technique. However, the fact that the wear rates of Ni-20Cr coatings under sliding and abrasion conditions (Fig. 13a, b) are substantially higher than Al_2O_3 and WC-Co coatings in spite of the higher toughness of Ni-20Cr coatings implies that the low hardness of Ni-Cr coatings as compared to Al_2O_3 and WC-Co coatings is responsible for its poor performance. In contrast to the above observation, the erosion rate of Ni-20Cr coatings is comparable to that of Al_2O_3 coatings and such a result can only be due to much higher toughness of Ni-Cr coatings as compared to Al_2O_3 coatings. Thus it can be concluded that while hardness of the coating is the predominant factor determining the sliding wear and abrasion resistance, an optimum combination of hardness and toughness provides the best erosion resistance.

However, the above analysis has disregarded the observation that while the hardness of Ni-Cr coatings decrease substantially with increasing particle size (Fig. 10), this effect is not manifested in terms of increased wear rate of Ni-Cr coatings (Fig. 13). Such a discrepancy can be related to the method of measurement of wear rate itself. In our experiments, we have measured the weight loss suffered by the sample and then converted it to volume loss using the density values of the coatings. Such a procedure is insensitive to the presence/absence of porosity in the coating, unless the measurement of thickness loss of the sample that would have been sensitive to porosity levels in the coating. Since the observed decrease in hardness of Ni-Cr coating with increasing particle size is actually a manifestation of porosity effect, it is not reflected in the wear data.

4. Conclusions

1. A decrease in powder particle size reduces the roughness and porosity in the case of Ni-Cr and Al_2O_3 coatings. However, in the case of WC-Co, the effect is marginal due to fact that the flow of the softer binder (Co) phase during the coating process tends to reduce the roughness and porosity especially when the coarser particle size is utilized.
2. The hardness of the Al_2O_3 coatings is primarily determined by the relative proportions of α and γ-Al_2O_3 phases and finer particles result in lower-coating hardness due to higher-volume fraction of the softer γ-Al_2O_3 phase. In the case of Ni-Cr, hardness is primarily influenced by porosity with the coatings formed with the coarser particles exhibiting lower hardness due to higher porosity. In the case of WC-Co coatings, particle size of the feedstock does not affect the coating hardness.
3. The toughness of the Al_2O_3 and WC-Co coatings are dependent on the presence of the harder but brittle phase W_2C in the case of WC-Co coatings and α-Al_2O_3 in the case of Al_2O_3 coatings. In the case of Al_2O_3, toughness decreases with increasing particle size since the proportion of γ-Al_2O_3 phase decreases with increasing particle size. In contrast, in the case of WC-Co, the proportion of brittle W_2C phase is higher at lower-particle sizes there by causing a decrease in toughness of the coating at lower-particle sizes.
4. The wear resistance (sliding wear, abrasion and erosion) of the WC-Co and Ni-Cr coatings is only marginally affected by the powder particle size. In the case of Al_2O_3 coatings, there is a clear trend of increasing abrasion and sliding wear resistance with increase in power particle size due to higher hardness resulting from lower fraction of γ-Al_2O_3. In contrast, the best erosion resistance is obtained at intermediate powder particle size since it results in the optimum combination of toughness and hardness.
5. Finally it can be concluded that given the marginal influence of powder particle size on coating properties and performance, there is really no need to alter the current philosophy of using commercial powders with broad particle size distribution (i.e., 10-44 μm) to form DSC (and HVOF) coatings.

Acknowledgments

The authors are grateful to Centre for Engineered Coatings Group for assisting in generation of the coated specimens and also to Material Characterization Group for kind assistance. The authors also thank the reviewers of this paper for their constructive comments which have certainly improved the quality.

References

1. T.N. Rhys-Jones, Thermally Sprayed Coating System for Surface Protection and Clearance Control Applications in Aero-Engines, *Surf. Cat. Technol.*, 1990, **43-44**, p 402-41
2. C.J.S. Guest, Plasma and Detonation Gun Coatings, *Trans IMF*, 1986, **64**, p 33-38
3. C.J. Li and A. Ohmori, The Lamellar Structure of Detonation Gun Sprayed Al_2O_3 Coating, *Surf. Cat. Technol.*, 1996, **82**, p 254-258
4. R.C. Tucker Jr., Structure Property Relationships in Deposits Produced by Plasma Spray and Detonation Gun Techniques, *J. Vac. Sci. Technol.*, 1974, **11**(4), p 725-734
5. J. Berget, E. Bardal, and T. Ronge, Effect of Matrix Composition and Particle Size on Structure and Erosion-Corrosion Resistance of HVOF Sprayed WC-Co-Cr Coatings. In T.S. Sudarshan, M. Jeandin and K.A. Khor (Eds.), *Surface Modification Technologies XI.*, London: The Institute of Materials, 1998, p 501-515

6. J. Berget, E. Bardal, and T. Ronge, Effects of Powder Composition on the Erosion, Corrosion and Erosion-Corrosion Properties of HVOF Sprayed WC Based Coatings, *Thermal Spray: Meeting the challenges of the 21st century*, C. Coddet, Ed. (Nice, France), ASM International, 1998, p 305
7. Chang-Jiu Li and Wen-Ya Li, Effect of Sprayed Powder Particle Size on the Oxidation behavior of MCrAlŸ Materials during High Velocity Oxygen-Fuel Deposition, *Surf. Coat. Technol.*, 2002, **162**, p 31-41
8. P. Cheang and K.A. Khor, Influence of Powder Characteristics on Plasma Sprayed Hydroxyapatite Coatings, *J. Thermal. Spray Technol.*, 1996, **5**, p 310-316
9. V. Kadyrov, M. Yakovlev, D. Sen, D. Srinivasa Rao, K.P. Rao, and A.V. Saibaba, Detonation Coating Process, *Trans. PMAI*, 1993, **20**, p 1-5
10. P. Saravanan, V. Selvarajan, D.S. Rao, S.V. Joshi, and G. Sundararajan, Influence of Process Variables on the Quality of Detonation Sprayed Alumina Coatings, *Surf. Coat. Technol.*, 2000, **123**, p 44-54
11. G. Sundararajan, G. Sivakumar, and D. Srinivasa Rao, The Interrelationship between Particle Velocity and Temperature, Splat Formation and Deposition Efficiency in Detonation Sprayed Alumina Coating, *Thermal Spray 2001: New Surfaces for New Millennium*. C.C. Berndt, K.A. Khor, and E.F. Lugscheider, Ed., May 28-30, 2001 (Singapore), ASM International,2001, p 849
12. G. Sivakumar, L. Ramakrishna, V. Jain, D. Srinivasa Rao, G. Sundararajan, and G. Madhusudhan Reddy, The Influence of the Process Parameters on the Properties of Detonation Sprayed WC-12%Co Coatings, *Thermalspray 2001: New Surfaces for New Millennium*, C.C. Berndt, K.A. Khor, E.F. Lugscheider, Ed., May 28-30, 2001 (Singapore), ASM International, 2001, p 1031
13. A.G. Evans and E.A. Charles, Fracture Toughness Determined by Indentation, *J. Am. Cem. Soc.*, 1976, **59**, p 371-372
14. K.R.C. Somaraju, D. Srnivasarao, G. Sivakumar, D. Sen, G.V.N. Rao, and G. Sundararajan, The Influence of Powder Characteristics on the Properties of Detonation Sprayed Cr_3C_2–25NiCr Coatings, *Thermal Spray: Surface Engineering via Applied Research*, C.C. Berndt, Ed. (Montreal Quebec Canada), ASM International, 2000, p 309
15. D.S. Arensburger, S.M. Zimakov, P.A. Kulu, and M.A. Oyaviir, Coatings Deposited by the High-Velocity Flame Spraying Method, *Pow. Met. Metal Cerms.*, 2001, **40**, p 127-134
16. R. McPherson, On the Formation of Thermally Sprayed Alumina Coatings, *J. Mat. Sci.*, 1980, **15**, p 3141-3149
17. Y. Gao, X. Xu, Z. Yan, and G. Xin, High Hardness Alumina Coatings Prepared by Low Power Plasma Spraying, *Sur. Coat. Technol.*, 2002, **154**, p 189-193
18. R. McPherson, Formation of Metastable Phases in Flame and Plasma-Prepared Alumina, *J. Mat. Sci.*, 1973, **8**, p 851-858
19. A. Kulkarni, J. Gutleber, S. Sampath, A. Goland, W.B. Lindquist, H. Herman, A.J. Allen, and B. Dowd, Studies of the Microstructure and Properties of Dense Ceramic Coatings Produced by High-Velocity Oxygen-Fuel Combustion Spraying, *Mat. Sci. Eng., A*, 2004, **369**, p 124-137
20. D. Nolan, P. Mercer, and M. Samandi, Microstructural Stability of Thermal Sprayed WC-Co Composite Coatings in Oxidizing Atmospheres at 450°C, *Sur. Eng.*, 1998, **14**, p 124-128
21. R. Schwetzke and H. Kreye, Microstructure and Properties of Tungsten Carbide Coatings Sprayed with Various HVOF Spray Systems, *Thermal Spray: Meeting the Challenges of the 21st Century*, C. Coddet, Ed., May 25-29, (Nice, France), ASM International, 1998, p 187
22. T. Kraak, W. Herlaar, J. Wolke, K. De Groot, and E.A. Hyduk Jr., Influence of Different Gases on the Mechanical and Physical Properties on HVOF Sprayed Tungsten Carbide Cobalt, *Thermal Spray: International Advances in Coatings Technology*, C.C. Berndt, Ed., May 25-June 5, 1992 (Orlando, FL), ASM International, 1998, p 153
23. V. Ramanath and N. Jayaraman, Characterization and Wear Performance of Plasma Sprayed WC-Co Coatings, *Mat. Sci. Tech.*, 1989, **5**, p 382-388
24. C.J. Li, A. Ohmori, and Y. Harada, Effect of Powder Structure on the Structure of Thermal Sprayed WC-Co Coatings, *J. Mat. Sci.*, 1996, **31**, p 785-794
25. T. Sundararajan, S. Kuroda, F. Abe, and S. Sodeoka, Effect of Thermal Cycling on the Adhesive Strength of Ni-Cr Coatings, *Surf. Coat. Technol.*, 2005, **194**, p 290-299
26. L. Rama Krishna, D. Sen, Y.S. Rao, G.V. Narasimha Rao, and G. Sundararajan, Thermal Spray Coating of Aluminum Nitride Utilizing the Detonation Spray Technique, *J. Mater. Res.*, 2002, **17**(10), p 2514-2523
27. T. Nakamura, G. Qian, and C.C. Berndt, Effects of Pores on Mechanical Properties of Plasma-Sprayed Ceramic Coatings, *J. Am. Ceram. Soc.*, 2000, **83**((3), p 578-584
28. J. Luo and R. Stevens, Porosity-Dependence of Elastic Moduli and Hardness of 3Y-TZP Ceramics, *Crem. Inter.*, 1999, **25**, p 281-286
29. C. Verdon, A. Karimi, and J.L. Martin, Microstructural and Analytical Study of Thermally Sprayed WC-Co Coatings in Connection with their Wear Resistance, *Mat. Sci. Eng. A*, 1997, **234-236**, p 731-734
30. B. Roebuck and E.A. Almond, Deformation and Fracture Processes and the Physical Metallurgy of WC-Co Hardmetals, *Int. Mat. Revs.*, 1988, **33**(2), p 90-110